Generation of high-dimensional energy-time-entangled photon pairs

Da Zhang, Yiqi Zhang, Xinghua Li, Dan Zhang, Lin Cheng, Changbiao Li, and Yanpeng Zhang*
Key Laboratory for Physical Electronics and Devices of the Ministry of Education & Shaanxi Key Lab of Information Photonic Technique, Xi'an Jiaotong University, Xi'an 710049, China
(Received 4 August 2017; published 22 November 2017)

High-dimensional entangled photon pairs have many excellent properties compared to two-dimensional entangled two-photon states, such as greater information capacity, stronger nonlocality, and higher security. Traditionally, the degree of freedom that can produce high-dimensional entanglement mainly consists of angular momentum and energy time. In this paper, we propose a type of high-dimensional energy-time-entangled qudit, which is different from the traditional model with an extended propagation path. In addition, our method mainly focuses on the generation with multiple frequency modes, while two- and three-dimensional frequency-entangled qudits are examined as examples in detail through the linear or nonlinear optical response of the medium. The generation of high-dimensional energy-time-entangled states can be verified by coincidence counts in the damped Rabi oscillation regime, where the paired Stokes–anti-Stokes wave packet is determined by the structure of resonances in the third-order nonlinearity. Finally, we extend the dimension to N in the sequential-cascade mode. Our results have potential applications in quantum communication and quantum computation.

DOI: 10.1103/PhysRevA.96.053849

I. INTRODUCTION

Correlation of entangled quantum particles is stronger than that allowed by classical physics. The correlation is one of the most deep foundational questions in quantum mechanics [1], and forms the basis of many emerging quantum technologies [2–5]. The most widespread technique for creating these quantum resources is spontaneous parametric down-conversion (SPDC) [6]. However, the inferiority of SPDC sources lies in the broad bandwidth determined by the phase-matching condition, which is usually on the order of several THz or hundreds of GHz. The broadband SPDC source becomes very dim in many applications requiring narrow-band photons, such as long-distance fiber optical quantum communication (∼GHz), strong interaction of the photons with atoms and molecules (∼MHz,), and interference of independent sources without time synchronization (∼GHz) [7]. Much effort has been used in the past more than one decades to narrow down the SPDC photon bandwidth by using optical cavities [8–10] and passive filtering [11]. However, the bandwidth of SPDC polarization-entangled photon pairs is still wider than most atomic transitions and leads to a very low efficiency of storing these polarization states in a quantum memory [9,12].

Due to their low decoherence rate, photons are used in many experiments as a robust carrier of entanglement. Recently, the Harris group [13,14] generated narrow-bandwidth time-frequency entangled paired photons with the two driving lasers running in continuous-wave mode, making use of electromagnetically induced transparency (EIT) [15] and spontaneous parametric four-wave mixing (SPFWM). Photons produced from this method not only possess narrow bandwidth but also automatically match the atomic transitions. The applications of these narrow-band photons include the demonstration of a single-photon memory with a storage efficiency of about 50% [16], a single-photon precursor [17], and quantum key distribution [18].

Meanwhile, in order to increase information carrying capacity, some scientists have been drawn to the production of photons that are simultaneously entangled in more than one degree of freedom, or hyper-entangled. But it is difficult to keep the stability of the system when different degrees of freedom are regulated. Another way to reach this goal is using high-dimensional (assume H dimension) two-photon entanglement, wherein each photon is an H-level qudit. From a fundamental standpoint, higher-dimensional entanglement implies stronger violations of locality [19,20] and is especially useful in the study of mutually unbiased bases in higher dimensions [21]. More relevant to practical applications, higher-dimensional entanglement provides increased security and robustness [22–24] and a higher information capacity [23,25,26].

The degrees of freedom of generally generated high-dimensional entangled biphoton states mainly include orbital angular momentum [27] and energy time [28]. For the orbital angular momentum, the generation mechanism mainly uses the spatial light modulator to allow the polarization of entangled two-photon states to carry orbital angular momentum so that the degree of freedom in the orbital angular momentum also has entanglement properties. Photon pairs with high-dimensional energy-time entanglement properties are generated primarily by extending the propagation path [29], which will lead to some drawbacks. With the increase of the path, the success rate of generating the high-dimensional energy-time-entangled state will decrease rapidly. Here, we propose a new method for producing high-dimensional energy-time-entangled photon pairs based on the four-level double-Λ EIT system, whose high-dimensional features originate from multiple frequency modes. Frankly speaking, the transverse effects in paired-photon generation by the four-level system has been discussed in detail [30,31]. Du *et al.* also discussed the correlation characteristics of two-photon states under the single transverse mode of the generating fields [32]. Compared with the previous double-Λ configurations, the extended frequency modes are mainly produced by the splitted atomic energy level induced by the dressing field, resulting in high-dimensional energy-time entanglement.

*ypzhang@mail.xjtu.edu.cn

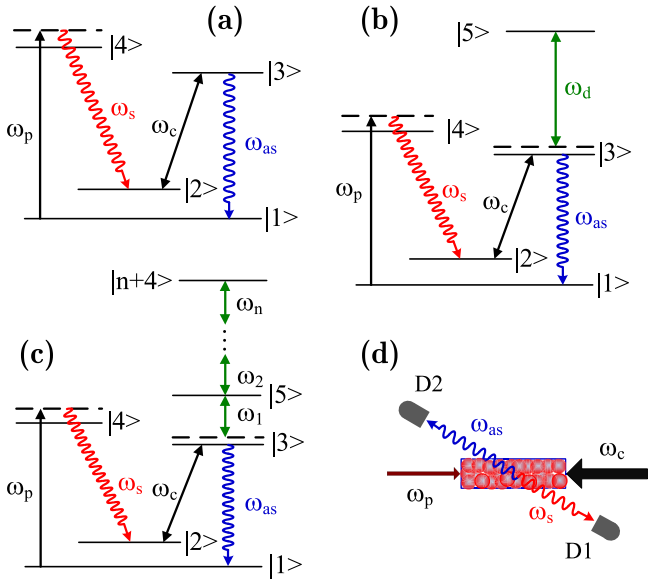

FIG. 1. Mechanisms of biphoton generation from a four-level system. In the presence of a cw pump ω_p and coupling ω_c beams, paired Stokes ω_s, and anti-Stokes ω_{as} photons are spontaneously created from the FWM processes in the low-gain regime. (a)–(c) No dressed field, single-dressed field, and N-dressed field cases, respectively. (d) The backward detection geometry for two-photon emission shown in (a), (b), and (c).

The paper is organized as follows. In Sec. II, we derive a general formalism of the two-photon state and biphoton wave packet generated from the FWM parametric process. In Sec. III, we show that the linear and nonlinear optical responses to the generated fields play an important role in determining the two-photon amplitude. By looking at the nonlinear susceptibility, we illustrate the mechanism of biphoton generation and how to extend to higher dimension. In Sec. IV we study the linear and nonlinear optical responses to the generated fields in the presence of an additional dressing field. We show that the frequency mode of generated fields have substantially increased with the existence of dressing field. In Sec. V, paired Stokes and anti-Stokes photons are studied in coincidence counting measurements. Theoretical analysis suggests that the two-photon temporal correlation has a significant difference in the presence and absence of the dressing field. In Sec. VI, according to the nonlinear response characteristics of the atomic medium, we extend the dimension of entanglement to N. Finally, we draw the conclusion and outlook in Sec. VII.

II. OVERVIEW OF TWO-PHOTON STATE FUNCTION

We begin with a medium of identical four-level atoms initially prepared in their ground level $|1\rangle$. The medium is confined within a long, thin cylindrical volume with a length L. The averaged atomic density is N. The schematic of biphoton generation via a four-level double-Λ atomic system is shown in Fig. 1(a). A simplified experimental setup for paired photon generation in such a four-level system is illustrated in Fig. 1(d), where a weak pump laser with angular frequency ω_p and a strong control field with angular frequency ω_c are counterpropagating through the medium. The weak pump beam is applied to the atomic transition $|1\rangle \rightarrow |4\rangle$ with a detuning $\Delta_p = \omega_{41} - \omega_p$, and a strong control laser is near the resonant frequency of the atomic transition $|2\rangle \rightarrow |3\rangle$, where ω_{ij} is the transition frequency between levels $|i\rangle$ and $|j\rangle$. Paired Stokes and anti-Stokes photons are spontaneously produced from the FWM process in the low-gain limit. As shown in Fig. 1(a), the strong coupling laser forms a standard three-level Λ EIT scheme with the generated anti-Stokes field. Therefore, the role of the coupling laser here is that it not only assists the FWM nonlinear process but also creates a transparency window for the anti-Stokes photons with the slow-light effect. For simplicity, in this paper we will not take into account the Doppler broadening and polarization effects. Since the control laser is much stronger than the pump and a large detuning puts the pump far off resonance, the quantum atomic noise may be suppressed and the atomic population is maintained primarily in the ground state. In the two-photon limit, the quantum Langevin noise introduces unpaired photons, which are not of interest here and so are ignored [33,34]. In addition, we concentrate on the two-photon temporal correlation.

In the interaction picture the effective interaction Hamiltonian for the FWM parametric process takes the form,

$$\hat{H}_I = \epsilon_0 \int_V d^3 r \chi^{(3)} E_p^{(+)} E_c^{(+)} E_{as}^{(-)} E_s^{(-)} + \text{H.c.}, \tag{1}$$

where V is the interaction volume illuminated by the pump and control beams together and H.c. stands for the Hermitian conjugate. $\chi^{(3)}$ is the third-order nonlinear susceptibility to the Stokes (or anti-Stokes) field defined by the nonlinear polarizability. $E_p^{(+)}$ and $E_c^{(+)}$ are the positive-frequency parts of the pump and couple field which are classical plane waves,

$$E_p^{(+)} = E_p e^{i(\hat{k}_p \cdot \hat{z} - \omega_p t)}, E_c^{(+)} = E_c e^{-i(\hat{k}_c \cdot \hat{z} + \omega_c t)}. \tag{2}$$

The z direction is assumed to be parallel to the pump longitudinal propagation. In the Hamiltonian (1) we ignore the reflections from the system surfaces and use the rotating-wave approximation. The generated Stokes and anti-Stokes photons are given by the quantized fields,

$$E_s^{(+)} = \sum_{\hat{k}_s} E_s \hat{a}_{\hat{k}_s} e^{i(\hat{k}_s \cdot \hat{r} - \omega_s t)},$$
$$E_{as}^{(+)} = \sum_{\hat{k}_{as}} E_{as} \hat{a}_{\hat{k}_{as}} e^{-i(\hat{k}_{as} \cdot \hat{r} + \omega_{as} t)}, \tag{3}$$

where $E_j = i\sqrt{\hbar \varpi_j / 2\varepsilon_0 n_j^2 V_q}$ and V_q is the quantization volume. Using Eqs. (2) and (3) and after integration, the Hamiltonian (1) can be rewritten as

$$\hat{H}_I = \frac{i\hbar}{2} \int d\omega_s d\omega_{as} \kappa \Phi(\Delta k L) H(\hat{\alpha}_s + \hat{\alpha}_{as}, \rho) \times \hat{a}_s^+ \hat{a}_{as}^+ e^{-i(\omega_p + \omega_c - \omega_s - \omega_{as})}, \tag{4}$$

where $\kappa = -i\sqrt{\varpi_s \varpi_{as}} \chi^{(3)} E_c E_p$ is the nonlinear parametric coupling coefficient; ϖ_{as} and ϖ_s are central frequencies of the anti-Stokes and Stokes fields, respectively. Here, because of the steep EIT dispersion profile, all the indices of refraction are taken as unity. $\Phi(\Delta k L)$ is the longitudinal detuning function, which is an integral about z from $-L$ to 0 over the length of

the medium,

$$\Phi(\Delta kL) = \frac{1 - e^{-i\Delta kL}}{i\Delta kL}, \tag{5}$$

where $\Delta k = k_c - k_p + k_s - k_{as}$ is the phase mismatch along the longitudinal axis. Note that $\Phi(\Delta kL)$ carries the information of phase mismatch in the longitudinal direction over the entire medium. The natural spectral width of the two-photon state may be determined by this longitudinal detuning function. $H(\hat{\alpha}_s + \hat{\alpha}_{as}, \rho)$ is called the transverse detuning function, which is the integral over the area A of the intersection of the beam cross section,

$$H(\hat{\alpha}_s + \hat{\alpha}_{as}, \rho) = \frac{1}{A}\int_A d^2\rho e^{-i(\hat{\alpha}_s + \hat{\alpha}_{as})\cdot\hat{\rho}}. \tag{6}$$

In Eq. (6) we have assumed that A is independent on z. $\hat{\alpha}_s$ and $\hat{\alpha}_{as}$ are transverse wave vectors of Stokes and anti-Stokes photons, respectively. $\hat{\rho}$ is in the transverse plane normal to the longitudinal axis $\hat{z}$. For large emission angles and long effective-interaction length, the properties of the two-photon state are mainly determined by the function $\Phi(\Delta kL)$. In the limit of a medium with infinite length and cross section, both Φ and H become δ functions. Combining with the energy conservation δ function, they form perfect phase-matching conditions $\hat{k}_c - \hat{k}_p + \hat{k}_s - \hat{k}_{as} = 0$. The natural spectral width of the biphoton wave packet determined by Φ can be manipulated by changing the group delay to traverse the medium. For example, subnatural-linewidth photon pairs have been generated in the cold atomic medium using the EIT to alter the phase matching, and the coherence time has exceeded up to 1.5 μs [35]. In most of the experiments the range of the transverse component of the wave number is limited by placing pin holes in the beams. On the other hand, the transverse correlation of entangled photons has important applications in quantum imaging [36] and quantum lithography [37]. In this paper, we focus on the temporal correlation of the two-photon state. To simplify the proceeding discussions, we presumed that the cross section of the pump and coupling beam are large enough so that diffraction effects may be ignored. Thus the transverse detuning function H becomes a δ function. The wave vectors are replaced by wave numbers.

Considering the weak nonlinear interaction, we can obtain the initial state of paired Stokes–anti-Stokes photons by the first-order perturbation theory in the interaction picture. It gives the photon state at the output surface approximately as a linear superposition of $|0\rangle$ and $|\Psi\rangle$, where $|0\rangle$ is the vacuum state. Because the vacuum is not detectable, from now on we ignore it and only consider the two-photon part. The biphoton state $|\Psi\rangle$ can be expressed as

$$\begin{aligned}|\Psi\rangle &= \frac{-i}{\hbar}\int_{-\infty}^{+\infty} dt\hat{H}_I|0\rangle \\ &= \int d\omega_{as}\kappa\Phi(\Delta kL)\hat{a}_s^+\hat{a}_{as}^+\delta(\omega_p + \omega_c - \omega_s - \omega_{as})|0\rangle \\ &= \int d\omega_{as}\kappa(\omega_{as}, \omega_p + \omega_c - \omega_{as})\Phi(\Delta kL)\hat{a}_s^+\hat{a}_{as}^+|0\rangle. \end{aligned} \tag{7}$$

In Eq. (7), the Dirac δ function comes from the time integral and states the energy conservation. The two-photon state is entangled in frequency and wave number. In frequency space, the entanglement is the result of the frequency phase-matching condition, which implies that the detection of a photon at frequency ω_{as} requires the detection of the other photon at frequency $\omega_p + \omega_c - \omega_s$. The state is also entangled with respect to the wave number since the $\Phi(\Delta kL)$ function cannot be factorized as a function of k_{as} times a function of k_s. In the general noncollinear case, the wave-number entanglement has implications for the spatial correlation of photon pairs [30–32].

In most experiments the two-photon correlation is the quantity of primary interest. To look at the two-photon properties from a four-level system, we start with a simple experiment of the photon coincidence counting measurement. We suppose that detector $D1$ detects photons with frequency ω_s while photons with frequency ω_{as} fire detector $D2$. Assuming perfect detection efficiency, the averaged two-photon coincidence counting rate is defined by

$$R_{cc} = \lim_{T\to\infty}\frac{1}{T}\int_0^T dt_s\int_0^T dt_{as}G^{(2)}M(t_s - t_{as}), \tag{8}$$

where

$$G^{(2)} = \langle\Psi|E_s^{(-)}E_{as}^{(-)}E_{as}^{(+)}E_s^{(+)}|\Psi\rangle.$$

In Eq. (8), $M(t_s - t_{as})$ is the coincidence window function, which is defined so that $M = 1$ for $|t_s - t_{as}| < t_{cc}$ and it goes to zero rapidly for $|t| > t_{cc}$. Generally speaking, t_{cc} is quite large and so we may take $M = 1$. Using Eq. (7), the second-order intensity correlation function can be written as

$$\begin{aligned}G^{(2)} &= \langle\Psi|E_s^{(-)}E_{as}^{(-)}E_{as}^{(+)}E_s^{(+)}|\Psi\rangle \\ &= |\langle 0|E_{as}^{(+)}E_s^{(+)}|\Psi\rangle|^2 = |B(\tau_s, \tau_{as})|^2, \end{aligned} \tag{9}$$

where $\tau_i = t_i - r_i/c$ and r_i is the optical path from the output surface of the medium to the ith detector. For simplicity, we choose $r_s = r_{as}$. In general, the function $B(\tau_s, \tau_{as})$ is referred to as the two-photon amplitude, or biphoton wave packet. By substituting Eqs. (3) and (7) into Eq. (9), one obtains

$$B(\tau_s, \tau_{as}) = \sum_{k_s}\sum_{k_{as}} W\chi^{(3)}(\omega_{as})\Phi'(\Delta kL)e^{-i(\omega_s\tau_s + \omega_{as}\tau_{as})}, \tag{10}$$

where $\Phi'(\Delta kL) = \Phi(\Delta kL)e^{ik_{as}L}$ and all the constants and slowly varying terms have been absorbed into W. Now converting the sums in Eq. (10) into integrals in the standard fashion $\sum_{k_j} \to V_q^{1/3}/(2\pi)\int d\omega_j/v_j$, one obtains

$$B(\tau_s, \tau_{as}) = \psi(\tau)e^{-i(\omega_p + \omega_c)\tau_s}, \tag{11}$$

where

$$\psi(\tau) = W_1\int d\omega_{as}\kappa(\omega_{as})\Phi'(\omega_{as})e^{-i\omega_{as}\tau}, \tag{12}$$

with the relative time delay $\tau = \tau_{as} - \tau_s$. The integral in Eq. (12) is a Fourier transform of the longitudinal detuning function times the profile of the third-order nonlinear

susceptibility. In general, the pattern of the two-photon amplitude is determined by both κ and Φ'.

III. OPTICAL RESPONSE OF A FOUR-LEVEL SYSTEM

The two-photon wave function is determined by both the nonlinear susceptibility and the longitudinal detuning function. Therefore, in this section we look at the linear and nonlinear optical responses to the generated fields. On one hand, the importance of the nonlinear susceptibility is that it not only characterizes the strength of the nonlinear parametric process but also is the mechanism of biphoton generation. As a consequence, it determines the feature of the two-photon temporal correlation in one regime. On the other hand, the longitudinal detuning function sets the natural spectral width of biphotons and governs the pattern of the temporal correlation in another regime. Using the probability amplitude model, the third-order nonlinear susceptibility for the generated anti-Stokes field is [30–32,38]

$$\chi^{(3)} = \frac{N\mu_{13}\mu_{24}\mu_{41}\mu_{32}}{\varepsilon_0\hbar^3(-\Delta_p + i\gamma_{14})[4(\omega + i\gamma_{13})(\omega + i\gamma_{12}) - |\Omega_c|^2]} = \frac{N\mu_{13}\mu_{24}\mu_{41}\mu_{32}}{\varepsilon_0\hbar^3 4(-\Delta_p + i\gamma_{14})(\omega - \Omega_e/2 + i\gamma_e)(\omega + \Omega_e/2 + i\gamma_e)}, \quad (13)$$

where μ_{ij} are the electric dipole matrix elements and γ_{ij} the dephasing rates. $\Omega_e = \sqrt{\Omega_c^2 - (\gamma_{13} - \gamma_{12})^2}$ is the effective coupling Rabi frequency, where γ_{12} and γ_{13} are dephasing rates of coherence $|3\rangle \to |1\rangle$ and $|2\rangle \to |1\rangle$. $\gamma_e = (\gamma_{12} + \gamma_{13})/2$ is the effective dephasing rate. We are interested in the optical response of the atomic dipoles oscillating at frequencies $\varpi_{as} + \omega$. The reason is that the resonances shown in the denominator of Eq. (13) will tell the generation mechanisms behind the FWM processes, e.g., how many modes can be generated for the Stokes and anti-Stokes fields and how these modes are correlated with each other [32,39–41]. The exact roots of the real part of the denominator in Eq. (13) are simple. There are two resonances, which occur at $\varpi_{as} + \Omega_e/2$ and $\varpi_{as} - \Omega_e/2$ with the associated linewidth γ_e. These two resonances correspond to two FWM processes existing in the system. The first FWM process happens when the central frequency of the anti-Stokes field is $\varpi_{as} + \Omega_e/2$ and the central frequency of the Stokes field is $\varpi_s - \Omega_e/2$. The other FWM occurs as the anti-Stokes field is peaked at $\varpi_{as} - \Omega_e/2$ while the Stokes field peaks at $\varpi_s + \Omega_e/2$. As expected, both FWMs satisfy the energy conservation $\omega_p + \omega_c - \omega_s - \omega_{as} = 0$. The spontaneously emitted paired photons propagate into opposite directions as shown in Fig. 1(d). On the other hand, in the case of strong coupling field power and low optical depth, the single-photon spectrum of anti-Stokes can be plotted in Fig. 2(a). The widths of these two resonance peaks are determined by $2\gamma_e$. The generated Stokes and anti-stokes photon pair can be described as the entanglement state with destructive interference $(|\varpi_{as} + \Omega_e/2\rangle|\varpi_s - \Omega_e/2\rangle - |\varpi_{as} - \Omega_e/2\rangle|\varpi_s + \Omega_e/2\rangle)/\sqrt{2}$.

The linear susceptibilities corresponding to the Stokes and anti-Stokes are

$$\chi_s = \frac{N\mu_{24}^2}{\varepsilon_0\hbar}\frac{4(\omega - i\gamma_{31})}{4(\omega - i\gamma_{21})(\omega - i\gamma_{31}) - |\Omega_c|^2}\frac{|\Omega_p|^2}{\Delta_p^2 + \gamma_{14}^2},$$
$$\chi_{as} = \frac{N\mu_{13}^2}{\varepsilon_0\hbar}\frac{4(\omega + i\gamma_{21})}{4(\omega + i\gamma_{21})(\omega + i\gamma_{31}) - |\Omega_c|^2}. \quad (14)$$

The linear susceptibilities χ_s and χ_{as} control the dispersion profile and transmission spectrum of the generated Stokes and anti-Stokes fields as they propagate through the medium. As a consequence, these linear susceptibilities will govern the natural spectral width of paired photons through the phase-matching condition. As described in Eq. (14), the standard Λ-type EIT exists in the generated anti-Stokes channel due to the strong coupling field E_c. The propagation constants of two weak fields within the medium are given by $k_{as} = (\varpi_{as} + \omega)/v_{as}$ and $k_s = (\varpi_s - \omega)/v_s$, respectively. v_{as} and v_s are group velocities of Stokes and anti-Stokes photons propagating through the system, which are defined by $v = c/[n + \omega(dn/d\omega)]$. $n(\omega)$ is the refractive index experienced by each weak field and is defined as $n = \sqrt{1 + \mathrm{Re}[\chi]}$. For the Stokes field, its group velocity approaches c because of $|\Omega_p|^2 \ll (\Delta_p^2 + \gamma_{14}^2)$. Accordingly, the group velocity of the anti-Stokes field is

$$v_{as} = \frac{c}{1 + \frac{\omega_{31}}{2}\frac{\mathrm{Re}[\chi_{as}(\omega)]}{d\omega}} = \frac{c}{1 + \frac{2\omega_{31}\mathrm{OD}\cdot\gamma_{31}}{k_{31}L|\Omega_c|^2}}, \quad (15)$$

where OD is optical depth. In the counterpropagating geometry, the resulting wave-number mismatch is

$$\Delta k = k_p - k_c + k_{as} - k_s = \left(\frac{1}{v_{as}} - \frac{1}{c}\right)\omega \approx \frac{\omega}{v_{as}}. \quad (16)$$

The bandwidth due to the group delay can then be estimated as $\Delta\omega_g \sim v_{as}/L$. On the other hand, the propagations of the Stokes and anti-Stokes beams are limited by the transmission spectral widths. It is known that the transmission spectral width is determined by the imaginary part of the linear susceptibility χ. Considering the situations here, the transmission profile plays the role only as the control field is near resonant with its transition. In such a case, the anti-Stokes transmission will be controlled by the EIT window as shown in Fig. 2(b). From the expression for the transmission $T(\omega) = e^{-\mathrm{Im}[\chi_{as}]kL}$, we can obtain the transmission bandwidth $\Delta\omega_t \approx |\Omega_c|^2/(\gamma_{31}\sqrt{\mathrm{OD}})$. From the above analysis, one can arrive at the conclusion that the competition between Ω_e, γ_e, and $\Delta\omega_g$ will determine which effect plays a dominant role in governing the feature of the two-photon correlation [32,39]. If the effective coupling Rabi frequency Ω_e and linewidths γ_e are smaller than the phase-matching bandwidth $\Delta\omega_g$, the two-photon amplitude are mainly determined by the nonlinear coupling coefficient. Instead, the slow-light effect can be used to dynamically control the biphoton temporal correlation time in the group-delay regime if $\Omega_e, \gamma_e > \Delta\omega_g$. In this region, the information of the two-photon spectrum is erased by the slow-light effect. To check the high-dimensional properties of energy time, we focus on the damped Rabi oscillation regime.

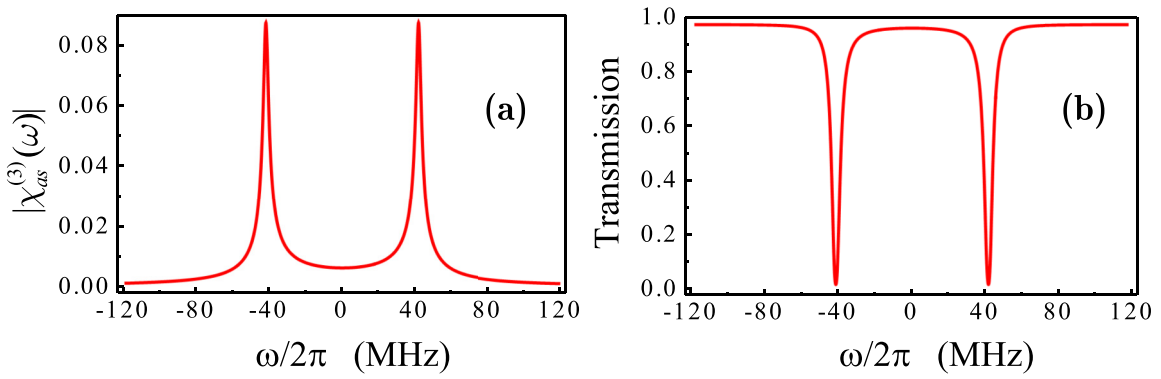

FIG. 2. (a) The doublet resonances shown in the third-order nonlinear susceptibility $|\chi^{(3)}|$ of the anti-Stokes beam. (b) Anti-Stokes transmission versus the detuning from the $|1\rangle \rightarrow |3\rangle$ transition in the presence of the coupling laser. The parameters used here are $\gamma_{13} = \gamma_{14} = 2\pi \times 3$ MHz, $\gamma_{12} = 0.01\gamma_{13}$, $\Delta_p = 50\gamma_{13}$, $\Omega_c = 30\gamma_{13}$, and OD = 10.

IV. OPTICAL RESPONSE OF MEDIUM WITH DRESSING FIELD

In this section, we will discuss the paired Stokes–anti-Stokes generation in a dressed five-level system as shown in Fig. 1(b). Comparing with the previous double-Λ schemes, the EIT effects offered in the current configuration may be manipulated by altering either the Rabi frequency of the control laser or the Rabi frequency of the dressing beam, or both. When the pump (E_p) and coupling (E_c) field are kept the same, a dressing laser with angular frequency ω_d is applied to the quantum transition $|3\rangle \rightarrow |5\rangle$ with a detuning $\Delta_d = \omega_{53} - \omega_d$. One may notice that two types of EIT exist in the system for the input probe beam, a ladder-type and a Λ-type, as shall be formally shown below. Again we will not take into account the Doppler broadening and polarization effects. By solving the probability amplitude model under this configuration, the third-order nonlinear susceptibility for the generated anti-Stokes field is

$$\chi'^{(3)} = \frac{N\mu_{13}\mu_{24}\mu_{41}\mu_{32}(\omega - \Delta_d + i\gamma_{53})}{2\varepsilon_0\hbar^3(\Delta_p - i\gamma_{14})D_1(\omega)},$$
$$D_1(\omega) = 4(\omega - \Delta_d + i\gamma_{53})(\omega + i\gamma_{21})(\omega + i\gamma_{31}) - |\Omega_d|^2(\omega + i\gamma_{21}) - |\Omega_c|^2(\omega - \Delta_d + i\gamma_{53}), \quad (17)$$

since the parametric conversion efficiency of twin beams is governed by the third-order nonlinear susceptibilities $\chi'^{(3)}$. The structure of these nonlinearities plays an important role in determining the feature of the biphoton wave packet. For example, as shown in Eq. (12), the integration over the full frequency spectrum will yield the two-photon spectral width around the residues. Comparing this width with that from the phase dispersion, a narrower one will play a major role in the biphoton wave packet. Solving the cubic function $\mathrm{Re}D_1(\omega) = 0$, one can find three roots which indicate a triplet of resonances. Figure 3(a) displays numerical simulations of three resonances. Alternatively, there are three types of FWM processes occurring in the interaction.

Since these three roots take very complicated forms, we divided them into two cases to discuss the following. (a) The intensity of the dressing field (E_d) is stronger than E_c, i.e., $\Omega_d \gg \Omega_c$. We can approximate $D_1(\omega)$ as $(\omega + i\gamma_{21}) \times [4(\omega - \Delta_d + i\gamma_{53})(\omega + i\gamma_{31}) - |\Omega_d|^2]$, which means the EIT effect mainly comes from the strong dressing field E_d not from the coupling field E_c. (b) The intensity of the dressing field (E_d) is weaker than E_c. In such a situation, $D_1(\omega)$ may be approximated as $(\omega - \Delta_d + i\gamma_{53}) \times [4(\omega + i\gamma_{21})(\omega + i\gamma_{31}) - |\Omega_c|^2]$. These two cases are equivalent in principle, so we just discuss the case (a). To visualize the optical responses of the medium to the generated Stokes and anti-Stokes fields in such a case, we rewrite Eq. (17) as

$$\chi_d^{(3)} = \frac{N\mu_{13}\mu_{24}\mu_{41}\mu_{32}(\omega - \Delta_d + i\gamma_{53})}{2\varepsilon_0\hbar^3(\Delta_p - i\gamma_{14})D_1'(\omega)},$$
$$D_1'(\omega) = (\omega + i\gamma_{21})[4(\omega - \Delta_d + i\gamma_{53})(\omega + i\gamma_{31}) - |\Omega_d|^2]. \quad (18)$$

By inspecting that the real part of $D_1'(\delta)$ vanishes, the triplet of resonances appears at

$$\omega_0 = 0, \omega_\pm = \frac{\Delta_d}{2} \pm \frac{\Omega_e'}{2}, \quad (19)$$

where $\Omega_e' = \sqrt{|\Omega_d|^2 + \Delta_d^2 - (\gamma_{53} - \gamma_{31})^2}$ and $\gamma_{e1} = (\gamma_{53} + \gamma_{31})/2$. The corresponding linewidths of the triplet of resonances are $\Gamma_0 = \gamma_{21}$ and $\Gamma_\pm = \gamma_{e1}$. Three types of FWMs appear behind $D_1'(\delta)$. Alternatively, three types of paired Stokes and anti-Stokes photons can be generated from these three FWM processes in the spontaneous emission region. One FWM process occurs when the central frequency of the anti-Stokes field coincides with the pump laser frequency ω_{31}, and the central frequency of the Stokes field coincides with the atomic-transition frequency $\omega_{41} - \Delta_p$. In this case, the correlated photon pairs are generated due to the absorption of a pair counter-propagating pump and coupling photons as required by the phase-matching conditions. The spontaneously emitted paired photons propagate into opposite directions. The second FWM occurs as the anti-Stokes field peaks at $\omega_{31} + \Delta_d/2 + \Omega_e'/2$ while the Stokes field peaks at $\omega_{41} - \Delta_p - \Delta_d/2 - \Omega_e'/2$. The third FWM exists when the anti-Stokes mode is centered at $\omega_{31} + \Delta_d/2 - \Omega_e'/2$ and

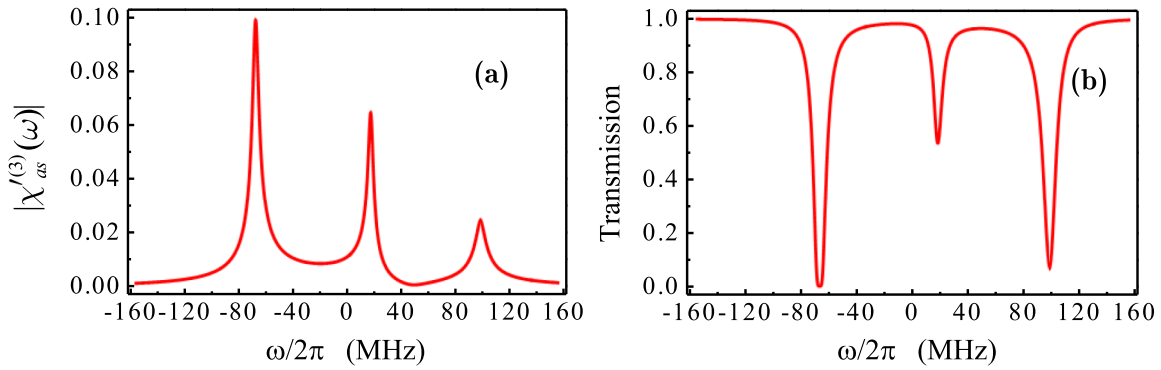

FIG. 3. (a) The triple resonances shown in the third-order nonlinear susceptibility $|\chi'^{(3)}|$ of the anti-Stokes beam. (b) Anti-Stokes transmission versus the detuning from the $|1\rangle \rightarrow |3\rangle$ transition in the presence of the coupling and dressing laser. The parameters used here are $\gamma_{13} = \gamma_{14} = 2\pi \times 3$ MHz, $\gamma_{53} = 2.3\gamma_{13}$, $\gamma_{12} = 0.01\gamma_{13}$, $\Omega_c = 40\gamma_{13}$, $\Omega_d = 50\gamma_{13}$, $\Delta_p = 50\gamma_{13}$, $\Delta_d = 20\gamma_{13}$, and OD = 10.

the Stokes mode is centered at $\omega_{41} - \Delta_p - \Delta_d/2 + \Omega'_e/2$. As expected, all three FWMs satisfy the energy conservation $\omega_p + \omega_c - \omega_s - \omega_{as} = 0$. Similarly, the generated photon pair can be described as the entanglement state,

$$|\Psi\rangle_1 = (d_1|\omega_{31}\rangle|\omega_{41} - \Delta_p\rangle - d_2|\varpi_{as} + \omega_+\rangle|\varpi_s - \omega_+\rangle - d_3|\varpi_{as} + \omega_-\rangle|\varpi_s - \omega_-\rangle),$$

where d_1,d_2, and d_3 satisfy $d_1^2 + d_2^2 + d_3^2 = 1$ and $d_1^2 - d_2^2 - d_3^2 = 0$ because of the normalization and destructive interference.

We can also understand the physical process from the dressed-state picture. In the presence of the on-resonance coupling field E_c, the levels $|2\rangle$ and $|3\rangle$ are split into two with a frequency separation equal to the coupling field Rabi frequency Ω_c as shown in Fig. 2(a). In such a case, two spontaneous FWM channels occur. When an additional dressing laser is applied to the quantum transition $|3\rangle \rightarrow |5\rangle$, the levels $|3\rangle$ and $|5\rangle$ will be splitted again, resulting in four eigenvalue and nondegenerate eigenstates accordingly. One of the trapping states is caused by the in-resonant coupling field. The single-photon spectrum of the anti-Stokes exhibits competitive behavior. If the intensity of the dressing field is greater than the coupling field, the single-photon spectrum shows the intensity of the central component greater than two sidebands and vice versa. It is worth noting that if the detunning of the dressing field is 0, i.e., the resonance situation, two of the four nondegenerate eigenstates are dark states in subsystems. On the other hand, focus on the linear optical response in Eq. (20), there only has two transmission channels for the sideband generation signals in electromagnetically induced transparency window and the central component will be completely absorbed. To pursue more frequency modes, the situation must be avoided. Therefore, there is a certain range of the detuning for the dressing field. When Δ_d is not equal to 0, the four nondegenerate eigenstates consist of one dark state and three bright states, making the double FWM channels into three FWM channels as shown in Fig. 3(a). Similarly, there are three transmission channels in the electromagnetically induced transparency window as shown in Fig. 3(b).

The linear susceptibilities at the Stokes and anti-Stokes can be written as

$$\chi_s^d = \frac{-N\mu_{24}^2/(\varepsilon_0\hbar)}{8\left[(\omega - i\gamma_{21}) + \frac{(\omega-\Delta_d-i\gamma_{53})|\Omega_c|^2}{|\Omega_d|^2-4(\omega-\Delta_d-i\gamma_{53})(\omega-i\gamma_{31})}\right]} \frac{|\Omega_p|^2}{\Delta_p^2 + \gamma_{14}^2},$$

$$\chi_{as}^d = \frac{N\mu_{13}^2}{\varepsilon_0\hbar} \frac{1}{\left[\frac{|\Omega_d|^2}{4(\omega-\Delta_d+i\gamma_{53})} + \frac{|\Omega_c|^2}{4(\omega+i\gamma_{31})} - (\omega + i\gamma_{21})\right]}. \quad (20)$$

As described in Eq. (20), two sets of EIT may exist in the generated ω_{as} channel. One is the standard Λ-type EIT due to the strong coupling E_c beam and the other is the ladder-type EIT due to the dressing laser E_d. There is a competitive relationship between the two EIT effects. As is mentioned in Sec. III, the linear susceptibilities will govern the natural spectral width of paired photons through the phase-matching condition. Instead, the high-dimensional energy-time entanglement photon pairs were born in such a regime that the two-photon amplitude was dominated by the nonlinear coupling coefficient. So we only consider the transmission in the anti-Stokes channel instead of the phase mismatch of FWM. Figure 3(b) is the anti-Stokes transmission via versus the detuning from the $|1\rangle \rightarrow |3\rangle$ transition in the presence of the coupling and dressing laser. There are three transmission windows corresponding to the three resonant positions of the $\chi'^{(3)}$. This means that the medium does not have a strong absorption for three types of FWM signals.

V. PHOTON COUNTING MEASUREMENT

In this section, we prove the generation of high-dimensional energy-time-entangled photon pairs by coincidence counting. We consider the case that the structure of the third-order nonlinear susceptibility $\chi^{(3)}$ mainly determines the profile of the biphoton wave packet. With a strong coupling laser and an optical depth of about 10, we work in the damped Rabi oscillation regime. In such a case, the longitudinal detuning function Φ is approximated to 1. The two-photon amplitude

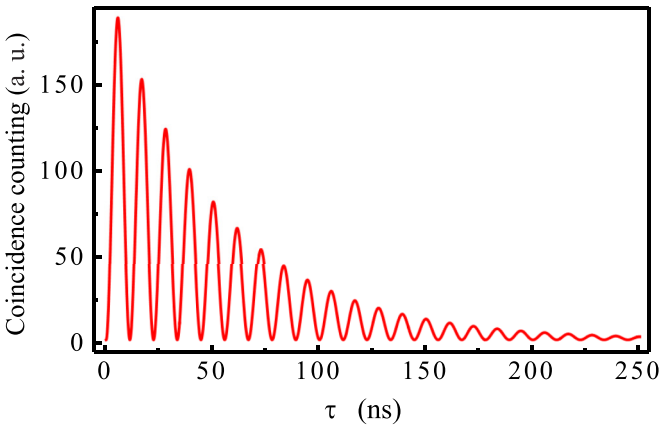

FIG. 4. The two-photon coincidence counting rate in the damped Rabi oscillation regime, where the paired Stokes–anti-Stokes wave packet is determined by the structure of double resonances shown in Eq. (13). The parameters here are the same as those used in Fig. 2.

in Eq. (11) now turns out to be the Fourier transform of $\chi^{(3)}$,

$$B(\tau) = \frac{N\mu_{13}\mu_{24}\mu_{41}\mu_{32}\sqrt{\varpi_s\varpi_{as}}}{4\varepsilon_0 c\hbar^3(-\Delta_p + i\gamma_{14})} E_p E_c e^{-i(\omega_p+\omega_c)\tau_s}, \int d\omega \frac{e^{-i\omega\tau}}{(\omega - \Omega_e/2 + i\gamma_e)(\omega + \Omega_e/2 + i\gamma_e)}. \quad (21)$$

By calculating the residues in Eq. (21), it gives

$$B(\tau_s,\tau_{as}) = \phi(\tau_s)\theta(\tau), \phi(\tau_s) = W_2 e^{-i(\omega_p+\omega_c)\tau_s}, \quad \theta(\tau) = (e^{i\Omega_e\tau/2} - e^{-i\Omega_e\tau/2})e^{(-\gamma_e\tau)}. \quad (22)$$

W_2 has absorbed all the constants and slowly varying terms. The physics of Eq. (22) is understood as follows. Since the two-photon state is entangled, it cannot be factorized into a function of τ_{as} times a function of τ_s. Equation (22) also shows destructive interference between the two biphoton channels. The first term in the second line on the right-hand side of Eq. (22) represents the two-photon amplitude of paired anti-Stokes at $\varpi_{as} + \Omega_e/2$ and Stokes at $\varpi_s - \Omega_e/2$, while the second term is the two-photon amplitude of paired anti-Stokes at $\varpi_{as} - \Omega_e/2$ and Stokes at $\varpi_s + \Omega_e/2$. Two-photon coincidence counting has the form,

$$R_{cc} = W_3[1 - \cos(\Omega_e\tau)]e^{-2\gamma_e\tau}, \quad (23)$$

where W_3 is a constant. Figure 4 is the numerical simulation two-photon coincidence counting rate in the damped Rabi oscillation regime, where the paired Stokes–anti- Stokes wave packet is determined by the structure of double resonances shown in $\chi^{(3)}$. The physics of Eq. (23) shows the beating between two types of paired photons generated from the two FWM processes. The two-photon correlation exhibits damped Rabi oscillations of period $2\pi/\Omega_e$. The damping rate is determined by the resonant linewidth γ_e in the doublet. In the two-photon coincidence counting experiment, the noise of coincidence counts is inevitable. They mainly result from the accidental coincidence between uncorrelated photons as the photon pairs are stochastically produced in time and space. Here, under the the interaction picture and perturbation theory, the evolution of the photon state describes clearly how biphotons are generated, but it's nearly helpless in the multiphoton events and accidental coincidences. To obtain the background noise of coincidence counting, we must transform the interaction picture to the Heisenberg picture. After that, the two-photon coincidence counting can be modified as

$$R'_{cc} = \langle E_s^{(-)} E_{as}^{(-)} E_{as}^{(+)} E_s^{(+)} \rangle = |B(\tau)|^2 + R_s R_{as},$$

where the $R_{as} R_s$ terms are independent of the time delay. They have the form,

$$R_s = \langle E_s^{(-)} E_s^{(+)} \rangle = R_{s0} \int d\omega |\chi^{(3)} \Phi(2\omega L/v_s)|^2,$$

$$R_{as} = \langle E_{as}^{(-)} E_{as}^{(+)} \rangle = R_{as0} \int d\omega |\chi^{(3)} \Phi(2\omega L/v_{as})|^2,$$

where R_{as0} and R_{s0} are constant.

Now, let's focus on the coincidence counting with the strong dressing case. In such a case, the two-photon amplitude has the form,

$$B_d(\tau) = \frac{N\mu_{13}\mu_{24}\mu_{41}\mu_{32}\sqrt{\varpi_s\varpi_{as}}}{2\varepsilon_0 c\hbar^3(\Delta_p - i\gamma_{14})} e^{-i(\omega_p+\omega_c)\tau_s} E_p E_c \int d\omega \times \frac{(\omega - \Delta_d + i\gamma_{53})e^{-i\omega\tau}}{(\omega + i\gamma_{21})(\omega + \omega_+ + i\gamma_{e1})(\omega + \omega_- + i\gamma_{e1})}. \quad (24)$$

After some mathematical calculations, one obtains

$$B_d(\tau_s,\tau_{as}) = W_d \phi_d(\tau_s)\theta_d(\tau), \ \phi_d(\tau_s) = e^{-i(\omega_p+\omega_c)\tau_s}, \quad \theta_d(\tau) = (i\gamma_{53} - i\gamma_{21} - \Delta_d)e^{-\gamma_{21}\tau} - e^{-\gamma_{e1}\tau}e^{-i\Delta_d\tau/2} \times \left[\Delta_d \cos(\Omega\tau) + \frac{3i\Delta_d^2}{4\Omega}\sin(\Omega\tau) - \Omega\sin(\Omega\tau)\right], \quad (25)$$

where $\Omega = \Omega'_e/2$. Again, all the slowly varying terms and constants have been absorbed into W_d. In Eq. (25), the approximation of $(\Delta_d, \Omega'_e) \gg (\gamma_{21} - \gamma_{e1}, \gamma_{53} - \gamma_{e1})$ is employed. Due to the triplet of resonances in $\chi'^{(3)}(\omega)$, the two-photon amplitude is the sum of three FWMs. It should be noted that since the bandwidth of the biphoton is smaller than the spectral width of the detectors, the coincidence counting rate is simply the module-squared two-photon amplitude. By using Eqs. (25) and (9), it is easy to find

$$R_{cc}^d = W_{d1}\left[e^{-2\gamma_{21}\tau} + e^{-2\gamma_{e1}\tau}\left[\cos^2(\Omega'_e\tau) + \left(\frac{3\Delta_d}{2\Omega'_e} - \frac{\Omega'_e}{2\Delta_d}\right), \sin^2(\Omega'_e\tau)\right] - \left[2\cos(\Omega'_e\tau)\cos\left(\frac{\Delta_d\tau}{2}\right) - \frac{\Omega'_e}{2\Delta_d}\sin(\Omega'_e\tau), \sin\left(\frac{\Delta_d\tau}{2}\right) + \frac{3\Delta_d}{\Omega'_e}\sin(\Omega'_e\tau)\sin\left(\frac{\Delta_d\tau}{2}\right)\right]e^{-(\gamma_{21}+\gamma_{e1})\tau}\right], \quad (26)$$

where W_{d1} is a constant. The physics of Eq. (26) is understood as follows: The destructive interference caused by three FWMs results in a damped oscillation in the two-photon joint detection probability. Note that the damping rate $2\gamma_{21}$ is very small, resulting in the coherent time of photon pairs greater than without the dressing field. Considering the presence of accidental coincidence in experiment, lower contours will be overwhelmed by uncorrelated background. As seen from

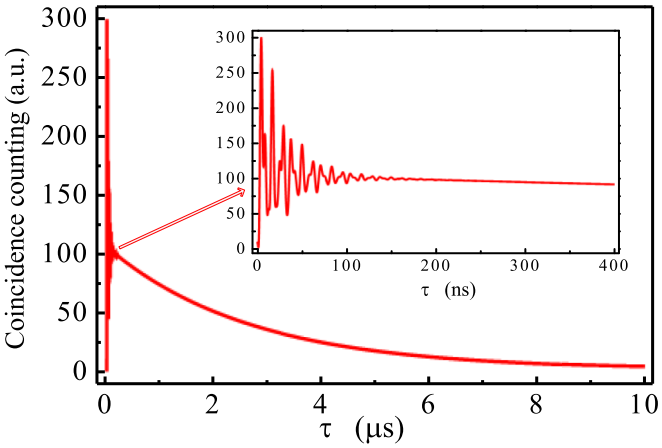

FIG. 5. The coincidence counting rate in the damped Rabi oscillation regime, where the two-photon wave packet is determined by the structure of triple resonances shown in Eq. (18). The parameters are the same as Fig. 3.

Eq. (26), the two-photon coincidences go to zero at $\tau = 0$ and $\tau \to \infty$. This indicates that a photon antibunching-like effect appears in R_{cc}^{d} due to the destructive interference between three FWMs. Figure 5 is the numerical simulation two-photon coincidence counting rate in the damped oscillation regime, where the paired Stokes–anti-Stokes wave packet is determined by the structure of triple resonances shown in $\chi_d^{(3)}$. In consideration of the background noise of coincidence counting, Eq. (26) can be modify as

$$R_{cc}^{dn} = R_{cc}^{d} + R_{s0}R_{as0}\int d\omega\left|\chi_d^{(3)}\Phi(2\omega L/v_s)\right|^2 \times \int d\omega\left|\chi_d^{(3)}\Phi(2\omega L/v_{as})\right|^2. \quad (27)$$

VI. EXTENSION TO *N* DIMENSIONS

Finally, we consider the sequential-cascade mode as shown in Fig. 1(c). In the case of the original configuration unchanged, the N-fold dressing field with angular frequency ω_j are applied to the transition $|j+3\rangle \to |j+4\rangle$ with detuning $\Delta_j = \omega_{(j+4)(j+3)} - \omega_j$. Similarly, we will not take into account the Doppler broadening and polarization effects. By solving the probability amplitude model under this configuration, the third-order nonlinear susceptibility for the generated anti-Stokes field is

$$\chi_{(as)}^{(3)} = \frac{N\mu_{13}\mu_{24}\mu_{41}\mu_{32}}{\varepsilon_0\hbar^3(\Delta_p - i\gamma_{14})} \times \frac{(\omega - \Delta_1 + i\gamma_{53})\cdots(\omega - \Delta_n + i\gamma_{(n+4)(n+3)})}{D_n(\omega)},$$

$$D_n(\omega) = 4(\omega + i\gamma_{21})(\omega + i\gamma_{31})(\omega - \Delta_1 + i\gamma_{53})\cdots(\omega - \Delta_n + i\gamma_{(n+4)(n+3)}) - |\Omega_c|^2(\omega + i\gamma_{21})(\omega - \Delta_1 + i\gamma_{53})\cdots(\omega - \Delta_n + i\gamma_{(n+4)(n+3)}) - \cdots - |\Omega_n|^2 \times (\omega + i\gamma_{21}), (\omega + i\gamma_{31})\cdots(\omega - \Delta_{n-1} + i\gamma_{(n+3)(n+2)}). \quad (28)$$

Next, we focus on the optical response of the atomic dipoles oscillating at frequencies $\varpi_{as} + \omega$. Since the roots are very complicated, we only carry out a phenomenological description. Think of D_2 as a polynomial about ω, it is obvious that D_2 has N roots and corresponds to N types of frequency modes $(\omega_1, \omega_2, \ldots \omega_N)$. Alternatively, N types of paired Stokes and anti-Stokes photons can be generated from these processes in the spontaneous emission region. The first FWM occurs as the anti-Stokes field peaks at $\varpi_{as} + \omega_1$ while the Stokes field peaks at $\varpi_s - \omega_1$. The second FWM exists when the anti-Stokes mode is centered at $\varpi_{as} + \omega_2$ and the Stokes mode is centered at $\varpi_s - \omega_2$ and so on. As expected, all N types of FWMs satisfy the energy conservation $\omega_p + \omega_c - \omega_s - \omega_{as} = 0$.

Accordingly, the entangled photon pair can be described as a form with destructive interference,

$$|\Psi\rangle_{as,s} = N_1|\varpi_{as} + \omega_1\rangle|\varpi_s - \omega_1\rangle - N_2|\varpi_{as} + \omega_2\rangle, \otimes|\varpi_s - \omega_2\rangle - \cdots\cdots - N_n|\varpi_{as} + \omega_N\rangle|\varpi_s - \omega_N\rangle, \quad (29)$$

where $N_1^2 + N_2^2 + \cdots + N_n^2 = 1$ and $N_1^2 - N_2^2 - \cdots - N_n^2 = 1$. This is a typical two-photon high-dimensional entangled state function. Traditional energy-time-entangled photon pairs usually increase the number of propagation paths to extend the dimension of entanglement. Their generation rate is inversely proportional to the number of paths. In our model, by introducing the dressing field to adjust the nonlinear response, the entangled photon pairs are generated with multiple frequency modes. Meanwhile, the proper absorption spectrum must ensure that the entangled photon pairs can be emitted from the surface of the medium.

VII. CONCLUSION

In conclusion, we extensively studied the optical properties of the paired Stokes and anti-Stokes generation in a four-level double-Λ system. To catch the physics instead of the complicated analysis, the Doppler broadening and polarization effects are not taken into account. The third-order nonlinear susceptibility shows that there are two types of FWMs that occur in the four-level system. To study the detailed information of the two types of biphoton generation, the nonlinear dominance of a two-photon wave packet is necessary, and the longitudinal detuning function approximates to 1. In the absence of the dressing field, the generated signal is a two-dimensional energy-time-entangled photon pair. Since the dressing field can modify the nonlinearity of the system, the nonlinear response of the system is exchanged. The nonlinear optical response increases when a dressing field acts on the system, resulting in an increase in the frequency modes of the generating signals. We examined the linear optical response of the medium to ensure that the generated signals are not strongly absorbed by the atomic system. In such a case, the generated signal becomes a three-dimensional energy-time-entangled photon pairs. This change can be verified from the two-photon coincidence counting experiment. Finally we pushed it to the case of the N-fold dressing, resulting in a higher-dimensional energy-time-entangled photon pair. Our method opens a window to test the locality along with the potential applications in quantum communication and quantum computation.

ACKNOWLEDGMENTS

The authors thank Jianming Wen for useful discussions. This work was supported by National Key R&D Program of China (Grant No. 2017YFA0303700), Natural Science Foundation of Shaanxi Province (Grant No. 2017JZ019), China Postdoctoral Science Foundation (Grant No. 2016M600777), National Natural Science Foundation of China (Grant No. 11474228), and Key Scientific and Technological Innovation Team of Shaanxi Province (Grant No. 2014KCT-10).

[1] A. Einstein, B. Podolsky, and N. Rosen, Phys. Rev. **47**, 777 (1935).
[2] T. B. Pittman, Y. H. Shih, D. V. Strekalov, and A. V. Sergienko, Phys. Rev. A **52**, R3429 (1995).
[3] D. V. Strekalov, A. V. Sergienko, D. N. Klyshko, and Y. H. Shih, Phys. Rev. Lett. **74**, 3600 (1995).
[4] L. Duan, M. D. Lukin, J. I. Cirac, and P. Zoller, Nature (London) **414**, 413 (2001).
[5] C. Weedbrook, S. Pirandola, R. Garciapatron, N. J. Cerf, T. C. Ralph, J. H. Shapiro, and S. Lloyd, Rev. Mod. Phys. **84**, 621 (2012).
[6] P. G. Kwiat, K. Mattle, H. Weinfurter, A. Zeilinger, A. V. Sergienko, and Y. Shih, Phys. Rev. Lett. **75**, 4337 (1995).
[7] M. Halder, A. Beveratos, N. Gisin, V. Scarani, C. Simon, and H. Zbinden, Nat. Phys. **3**, 692 (2007).
[8] Z. Ou and Y. Lu, Phys. Rev. Lett. **83**, 2556 (1999).
[9] X.-H. Bao, Y. Qian, J. Yang, H. Zhang, Z.-B. Chen, T. Yang, and J.-W. Pan, Phys. Rev. Lett. **101**, 190501 (2008).
[10] J. Fekete, D. Rieländer, M. Cristiani, and H. de Riedmatten, Phys. Rev. Lett. **110**, 220502 (2013).
[11] M. Halder, S. Tanzilli, H. de Riedmatten, A. Beveratos, H. Zbinden, and N. Gisin, Phys. Rev. A **71**, 042335 (2005).
[12] H. Zhang, X.-M. Jin, J. Yang, H.-N. Dai, S.-J. Yang, T.-M. Zhao, J. Rui, Y. He, X. Jiang, F. Yang, G.-S. Pan, Z.-S. Yuan, Y. Deng, Z.-B. Chen, X.-H. Bao, S. Chen, B. Zhao, and J.-W. Pan, Nat. Photon. **5**, 628 (2011).
[13] V. Balić, D. A. Braje, P. Kolchin, G. Y. Yin, and S. E. Harris, Phys. Rev. Lett. **94**, 183601 (2005).
[14] P. Kolchin, S. Du, C. Belthangady, G. Y. Yin, and S. E. Harris, Phys. Rev. Lett. **97**, 113602 (2006).
[15] S. E. Harris, Phys. Today **50**, 36 (1997).
[16] S. Zhou, S. Zhang, C. Liu, J. F. Chen, J. Wen, M. M. T. Loy, G. K. L. Wong, and S. Du, Opt. Express **20**, 24124 (2012).
[17] S. Zhang, J. F. Chen, C. Liu, M. M. T. Loy, G. K. L. Wong, and S. Du, Phys. Rev. Lett. **106**, 243602 (2011).
[18] C. Liu, S. Zhang, L. Zhao, P. Chen, C. H. F. Fung, H. F. Chau, M. M. T. Loy, and S. Du, Opt. Express **21**, 9505 (2013).
[19] D. Collins, N. Gisin, N. Linden, S. Massar, and S. Popescu, Phys. Rev. Lett. **88**, 040404 (2002).
[20] A. C. Dada, J. Leach, G. S. Buller, M. J. Padgett, and E. Andersson, Nat. Phys. **7**, 677 (2011).
[21] M. Wieśniak, T. Paterek, and A. Zeilinger, New J. Phys. **13**, 053047 (2011).
[22] H. Bechmann-Pasquinucci and A. Peres, Phys. Rev. Lett. **85**, 3313 (2000).
[23] H. Bechmann-Pasquinucci and W. Tittel, Phys. Rev. A **61**, 062308 (2000).
[24] L. Zhang, C. Silberhorn, and I. A. Walmsley, Phys. Rev. Lett. **100**, 110504 (2008).
[25] S. P. Walborn, D. S. Lemelle, M. P. Almeida, and P. H. S. Ribeiro, Phys. Rev. Lett. **96**, 090501 (2006).
[26] P. B. Dixon, G. A. Howland, J. Schneeloch, and J. C. Howell, Phys. Rev. Lett. **108**, 143603 (2012).
[27] D.-S. Ding, W. Zhang, Z.-Y. Zhou, S. Shi, G.-Y. Xiang, X.-S. Wang, Y.-K. Jiang, B.-S. Shi, and G.-C. Guo, Phys. Rev. Lett. **114**, 050502 (2015).
[28] A. Cabello, A. Rossi, G. Vallone, F. De Martini, and P. Mataloni, Phys. Rev. Lett. **102**, 040401 (2009).
[29] D. Richart, Y. Fischer, and H. Weinfurter, Appl. Phys. B **106**, 543 (2012).
[30] J. Wen and M. H. Rubin, Phys. Rev. A **74**, 023808 (2006).
[31] J. Wen and M. H. Rubin, Phys. Rev. A **74**, 023809 (2006).
[32] S. Du, J. Wen, and M. H. Rubin, J. Opt. Soc. Am. B **25**, C98 (2008).
[33] L. Zhao, Y. Su, and S. Du, Phys. Rev. A **93**, 033815 (2016).
[34] C. H. R. Ooi and M. O. Scully, Phys. Rev. A **76**, 043822 (2007).
[35] L. Zhao, X. Guo, C. Liu, Y. Sun, M. M. T. Loy, and S. Du, Optica **1**, 84 (2014).
[36] A. F. Abouraddy, B. E. A. Saleh, A. V. Sergienko, and M. C. Teich, Phys. Rev. Lett. **87**, 123602 (2001).
[37] A. N. Boto, P. Kok, D. S. Abrams, S. L. Braunstein, C. P. Williams, and J. P. Dowling, Phys. Rev. Lett. **85**, 2733 (2000).
[38] D. A. Braje, V. Balić, S. Goda, G. Y. Yin, and S. E. Harris, Phys. Rev. Lett. **93**, 183601 (2004).
[39] J. Wen, S. Du, and M. H. Rubin, Phys. Rev. A **75**, 033809 (2007).
[40] J. Wen, S. Du, and M. H. Rubin, Phys. Rev. A **76**, 013825 (2007).
[41] J. Wen, S. Du, Y. Zhang, M. Xiao, and M. H. Rubin, Phys. Rev. A **77**, 033816 (2008).